STATISTICS, OPTIMIZATION AND INFORMATION COMPUTING
Stat., Optim. Inf. Comput., Vol. **16**, December 2026, pp 6150–6166.
Published online in International Academic Press (www.IAPress.org)

Alcohol Use Disorder Detection and Classification from EEG Signals Using 2D Wavelet Transform, Machine Learning and Deep Learning

Achmad Rizal[1,*], Donny Setiawan Beu[1], Inung Wijayanto[1], Amira J. Zaylaa[2], Ayu Sekar Safitri[1]

[1]*School of Electrical Engineering, Telkom University, Bandung, Indonesia; achmadrizal@telkomuniversity.ac.id, donnysbeu@student.telkomuniversity.ac.id, iwjayanto@telkomuniversity.ac.id, ayusekarass@student.telkomuniversity.ac.id*
[2]*Electric and Computer Engineering Department, Faculty of Engineering, Beirut Arab University, Debbieh, Lebanon; a.zaylaa@bau.edu.lb*

Abstract Alcohol Use Disorder (AUD) is a psychological condition in which individuals lose control over alcohol consumption despite awareness of its harmful consequences. Electroencephalogram (EEG) signals offer a noninvasive means to characterize brain activity and have shown potential for distinguishing alcoholic and non-alcoholic subjects. However, highly accurate and automated detection methods for AUD remain limited. This study aims to improve classification performance using multichannel EEG signals transformed through time–frequency analysis combined with machine learning (ML) and deep learning (DL) techniques. Sixty-four–channel EEG recordings were converted into images and processed using a three-level Discrete Wavelet Transform (DWT). Statistical features were extracted from each wavelet sub-band and classified using various ML and DL models. Experimental results on real EEG data demonstrate that the Random Forest classifier achieves the highest accuracy of 93.77%, outperforming other methods. Comparative analysis indicates competitive performance relative to prior studies. These findings highlight the effectiveness of 2D DWT for EEG-based AUD detection and suggest that further improvements may be achieved through alternative mother wavelet selection, decomposition levels, and advanced classification techniques.

Keywords Alcohol Use Disorder, Deep Learning, Discrete Wavelet Transform, EEG signal, Machine Learning

DOI: 10.19139/soic-2310-5070-3819

1. Introduction

Alcohol Use Disorder (AUD) is regarded as a psychological predicament wherein an individual relinquishes command over their inclination to partake in alcoholic beverages, despite being cognizant of its detrimental effects on their well-being [1]. In the context of modern societies, the prevalence of alcohol problems has become a severe concern in public health. According to a report from the World Health Organization (WHO), globally, each year, approximately 3 million deaths are recorded that can be traced to high-risk alcohol consumption, accounting for about 5.3% of total deaths [2, 3]. In the context of medical research, long-term alcohol use is associated with impaired human brain development. At the same time, short-term consumption can trigger temporary effects such as memory impairment, loss of consciousness, impulsive behavior, poor judgment, and other impacts [4] as a representation of a series of fluctuating field potentials generated by the simultaneous activity of a large number of neurons [5]. EEG signals provide invaluable information about brain conditions, including neuron activity and wave patterns [6]. In the context of medical research, EEG signal analysis is used to understand various health disorders, including alcohol abuse [7, 8].

*Correspondence to: Achmad Rizal (Email: achmadrizal@telkomuniversity.ac.id). School of Electrical Engineering, Telkom University, Bandung, Indonesia.

ISSN 2310-5070 (online) ISSN 2311-004X (print)
Copyright © 2026 International Academic Press

Research on automatic alcoholic EEG has been carried out using various methods. One of the methods applied is wavelet transformation (WT). Ekaputri et al. [9] reported that the application of Multilevel Wavelet Packet Entropy (MWPE) to 1-dimensional alcoholic EEG signals produced an accuracy value of 77.8%. In addition, other research used Discrete Wavelet Transform (DWT) [7] to calculate sub-band coefficients from the analyzed EEG signal. Statistical parameters were applied from the selected wavelet coefficients, resulting in an accuracy of 95.6%. Other research utilizes the Dual-Tree Complex Wavelet Transform [8] by using two norms (L2Ns) and log-energy entropies (LEEs) extraction, resulting in a high level of accuracy, reaching 97.91%.

Another approach using a signal processing method by assuming N channel EEG as a two-dimensional (2D) image has been tested by Beu et al. [10]. This research was carried out by analyzing the texture of alcoholic EEG signals converted into 2D. The accuracy obtained was 93.77%. Barus et al. converted EEG signals into 2D and applied grey level difference matrix (GLDM) as feature extraction [11]. An accuracy of 75.25% was obtained using the natural gradient boosting (NGBoost) method for probabilistic prediction. However, wavelet decomposition on images converted from N-channel EEG signals has never been done. This provides an opportunity to explore the N-channel EEG signal further.

The research aims to improve the accuracy of image classification from multichannel EEG signals by utilizing time-frequency analysis, along with the Machine Learning (ML) and Deep Learning (DL) algorithms. The objective is to transform alcoholic EEG signals into a 2D format, enabling the processing of these signals as images. Then 2D DWT is used to decompose the resulting image, where statistical features are extracted. As for classification methods, both machine learning and deep learning techniques are employed. The anticipated outcome of this approach is the provision of a crucial contribution to the comprehension of brain activity patterns in EEG signals through time-frequency analysis. Our time-frequency analysis is expected to uncover additional information that was not previously detected by existing analysis methods. The classification methods and their implementation details are described in Section 2.

The main contributions of this study are threefold. First, unlike prior work that applies wavelet decomposition channel-by-channel, this study proposes a joint multichannel representation in which all EEG channels are stacked into a single two-dimensional array and decomposed simultaneously via 2D-DWT, so that a single wavelet decomposition covers all channels at once instead of repeating the decomposition per channel. Second, four complementary first- and second-order statistical descriptors (Energy, Entropy, Mean, and Standard Deviation) are systematically extracted from every DWT sub-band and benchmarked across five widely used ML and DL classifiers under an identical feature space, enabling a controlled comparison between classical and deep learning approaches. Third, the pipeline is evaluated under two independent data-partitioning ratios to provide an initial indication of the stability of the reported classification performance with respect to the amount of available training data.

2. Materials and Methods

The proposed AUD detection and classification design of the proposed method is provided in the block diagram shown in Figure 1. Starting from the group of candidates and the target being the human brain passing through the signal processing, conversion and decomposition, reaching to the feature extraction when needed and the automatic classification.

2.1. EEG Dataset

The nature of the data explored in the study is an electrical signal, i.e. EEG signal datasets. EEG signals were obtained from the ML Repository at the University of California, Irvine (UCI) [12, 13], which had previously been utilized in research [9]. A total of 120 participants were involved in the exploratory study. The total was split into two groups: the control group and the alcoholic group. The public UCI EEG repository comprises recordings from 122 subjects in total. Two subjects were excluded from the present analysis due to incomplete channel recordings, resulting in the 120 participants used in this study. Trials were partitioned into training, validation, and testing subsets at the trial level following the same subset of this dataset used in our related prior work [10].

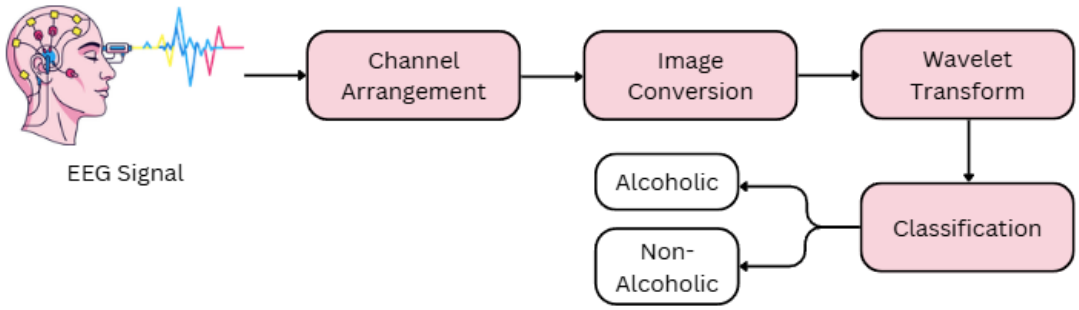


Figure 1. The proposed methods for EEG classification into Alcoholic and Non-Alcoholic. The pipeline consists of four stages: (1) Channel Arrangement, in which the raw multichannel EEG signal is organized into a channel-by-sample matrix; (2) Image Conversion, in which the matrix is rescaled to an 8-bit grayscale image via Min-Max scaling (Equation (1)); (3) Wavelet Transform, in which the resulting image is decomposed via 2D-DWT and statistical features are extracted from the sub-bands; and (4) Classification, in which the extracted features are fed into ML/DL classifiers to produce the Alcoholic / Non-Alcoholic decision.

Every participant completed 120 trials with two distinct stimuli. The stimulus is given under appropriate conditions, where S1 is identical to S2, or under inappropriate conditions, where S1 differs from S2. The dataset representation of the explored groups is shown in Figure 2, (a) for Alcoholic candidates and (b) for non-Alcoholic candidates.

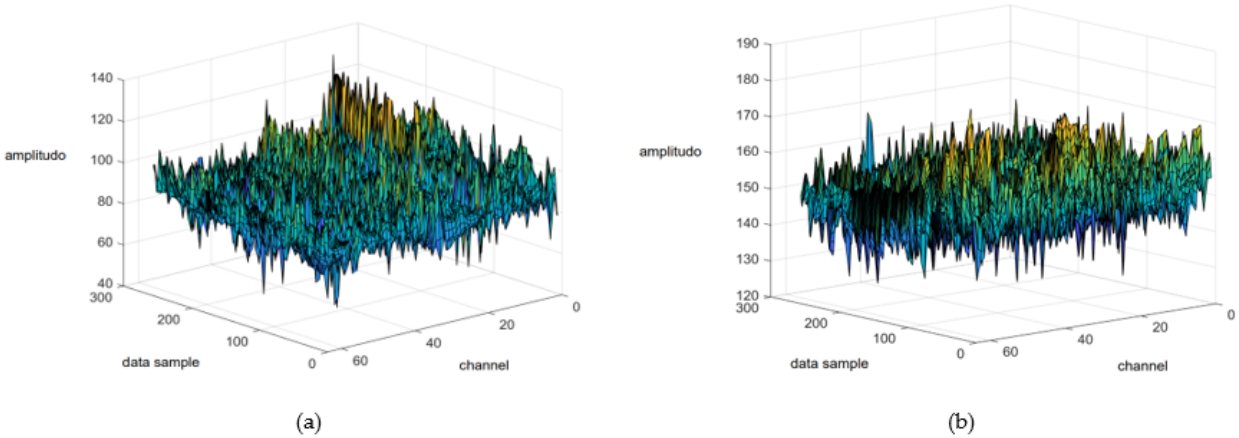


Figure 2. Dataset representation of the explored groups. (a) Dataset of Alcoholic candidates (b) Dataset of non-Alcoholic candidates.

The UCI EEG dataset was selected over other publicly available alcoholism-EEG datasets because it is freely accessible, provides raw 64-channel recordings (rather than pre-extracted features only), and has been used as a common benchmark in several closely related prior studies [9, 10, 11], which enables a direct comparison of the proposed method against the literature summarized in Table 3. The resulting dataset used in this study is approximately balanced between the alcoholic and control groups. Beyond the Min-Max scaling described in Section 2.3, no additional signal filtering, artifact removal, or baseline correction was applied to the raw recordings in this study; the 2D-DWT decomposition and the statistical feature extraction were applied directly to the min-max-scaled image representation. The 2D-DWT decomposition was implemented in Python using the PyWavelets library, with classical machine learning classifiers (KNN, SVM, Random Forest) implemented via scikit-learn and the deep learning classifiers (ANN, CNN) implemented using TensorFlow/Keras.

2.2. EEG Signal Processing

Signal processing commences by undertaking channel adjustments on the EEG signal channel, leading to the formation of N-channel $\times$ data samples. Subsequently, the value of the signal sample was altered to be tantamount to the image, with a range of values spanning from 0 to 255. Moreover, DWT and feature extraction methodologies were implemented by means of statistics. The ultimate phase entails the utilization of ML and DL in the classification procedure. Elaboration on the aforementioned steps can be found on Figure 1.

2.3. Dataset Conversion

EEG signals emanating from 64-channels were represented as a matrix of dimension: 64×256, where the 256-sample dimension corresponds to the native 1-second epoch length of each trial in the UCI EEG dataset, sampled at 256 Hz [12]. This study converted them into more understandable visual representations [14]. EEG signals were denoted: $X(m, n)$, where m is the number of channels and n the number of samples. $X(m, n)$ underwent a conversion process through Min-Max scaling, as described in Equation (1).

$$Z(m,n) = \text{int}\left(\frac{X(m,n) - X_{min}}{X_{max} - X_{min}}\right) \cdot 255 \tag{1}$$

The result of the scaling process produced an $m \times n$ image, where each pixel element has a value ranging from 0 to 255. This concept is equivalent to an 8-bit deep grayscale image, delivering rich visualizations and complying with digital image representation standards. This transformation facilitates research into the context of image signal processing.

In this representation, the 64 rows of the resulting image correspond to the 64 recording channels arranged in the fixed channel order provided by the UCI EEG dataset files, while the 256 columns correspond to consecutive time samples of each channel. This channel-stacking scheme does not explicitly preserve the two-dimensional scalp topology defined by the electrode montage; rows corresponding to physically adjacent electrodes are not guaranteed to be adjacent in the resulting image, and 2D-DWT may therefore treat physically distant electrodes as immediate neighbors at row boundaries. In this study, 2D-DWT is used primarily as a joint time–channel decomposition tool that captures shared frequency structure across channels, and the resulting sub-band statistics are treated as texture descriptors of the multichannel signal rather than as spatially calibrated maps of scalp activity.

2.4. Discrete Wavelet Transformation (DWT)

2D-DWT is a process in which an image is decomposed based on the frequency value of the image's subband [15]. DWT helps in retrieving information from the alcoholic EEG signals that have already been converted into images. DWT extracts wave coefficients that help analyze brain characteristics in greater depth. This process involves converting images from the spatial domain to the frequency domain [16], which can provide a more detailed understanding of the frequency patterns contained in the EEG data.

The image was broken down into sub-images through a three-level (level-1 to level-3) decomposition. At each level, the image is decomposed into four sub-bands, namely LL, LH, HL, and HH, representing special sub-bands in DWT analysis [17, 18] as shown in Figure 3. LL denotes the approximation sub-band (low-frequency content in both dimensions), whereas LH, HL, and HH denote the horizontal, vertical, and diagonal detail sub-bands, respectively; at each subsequent level, the decomposition is applied recursively to the LL sub-band of the previous level, so that a three-level decomposition yields ten sub-bands in total (LL3, and LH/HL/HH at levels 1, 2, and 3).

This study used the Daubechies 8 wavelet (db8) as a mother wavelet with three decomposition levels, in order to divide the 2D EEG signal into three levels to visualize the pulse. After decomposition features were extracted.

Daubechies wavelets were selected because they are orthogonal, compactly supported, and offer a favorable trade-off between smoothness and time–frequency localization, properties that make them widely used for EEG and biomedical signal decomposition [15, 17]; db8 in particular provides a higher number of vanishing moments than lower-order Daubechies wavelets (e.g., db2, db4), which improves its ability to represent smooth signal trends while still capturing transient details. A systematic comparison against other mother wavelets and decomposition depths was not performed in the present study and is identified as future work (see Section 5). Regarding the validity

of applying a three-level 2D-DWT to a 64×256 image, each decomposition level halves both dimensions of the approximation sub-band, from 64×256 at the input to 32×128 at level 1, 16×64 at level 2, and 8×32 at level 3. The db8 filter has 16 taps, which exceeds the channel dimension of 8 reached at the third level. The decomposition remains computable through standard boundary extension such as symmetric padding, as is common practice in wavelet toolboxes, though the relatively small channel dimension at the deepest level increases the influence of boundary effects on the level-3 sub-bands. Quantifying this effect, e.g., by comparing decomposition depth against reconstruction error or against a shallower two-level decomposition, is left for future work.

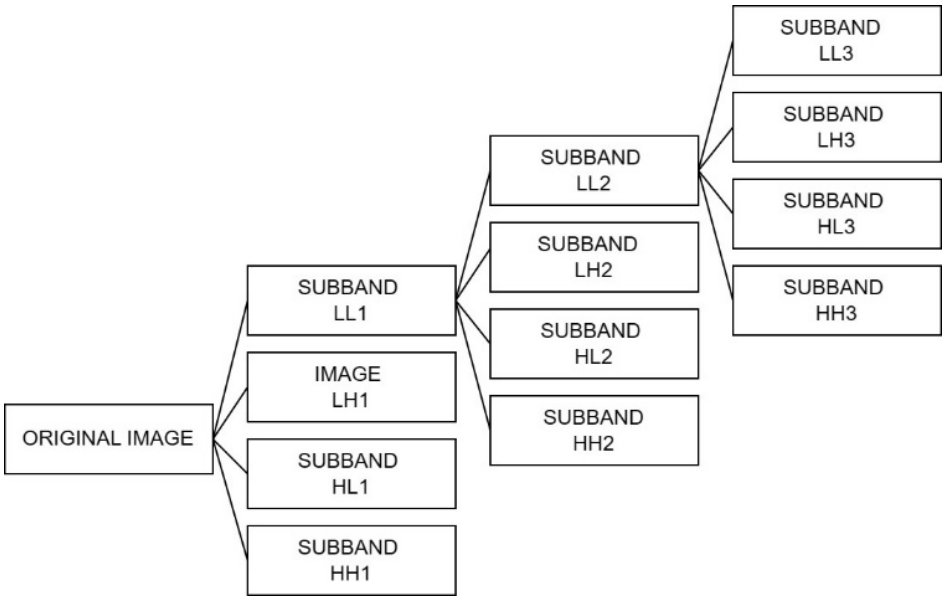


Figure 3. Illustration of the 3-level Discrete Wavelet Transform.

2.5. Feature Extraction

The extraction of features is a procedure that encompasses the emphasis of signal characteristics that possess a significant degree of dominance and discrimination [18]. Feature extraction aims to generate new features from the original data, providing significant benefits to reduce resource requirements for processing, without sacrificing feature data that has relevance [19]. One method of trait extraction is statistical feature extraction. This study employs the following parameters: Energy, Entropy, Mean and Standard Deviation as reported in Table 1 [20, 21].

The parameters are reported in Table 1, are of the first and second order statistical features that is formulated in Equation (2) to Equation (5). Combining essential information about signals (orders one and two) through feature extraction methods can improve understanding of the essential features of the explored signals. Thereby, adding knowledge about the distribution of pixel values and providing an overview of variation patterns that can be utilized for further analysis. Then features were fed into specific classifiers.

Energy, Entropy, Mean, and Standard Deviation were selected because they jointly capture complementary first- and second-order statistical properties of each wavelet sub-band, namely overall signal power (Energy), distributional randomness or texture complexity (Entropy), central tendency (Mean), and dispersion (Standard Deviation), and have been consistently reported as effective and computationally inexpensive descriptors in prior wavelet-based EEG and image-texture studies [20, 21]. Higher-order descriptors such as skewness and kurtosis, as well as automated feature selection or dimensionality-reduction procedures (e.g., Principal Component Analysis or Recursive Feature Elimination), were not applied in the present study, in order to keep the feature set small, interpretable, and directly comparable across all five classifiers; incorporating such descriptors and selection

procedures is a natural extension for future work, particularly to mitigate the feature redundancy observed for the "All Features" configuration reported in Section 3.

Table 1. The features extracted in the AUD detection and classification.

Parameter	**Equation**	**Significance**
Energy	$\sum_{i=1}^{N} x_i^2$ (2)	It explains how information is measured when using a probability frame.
Entropy	$-\sum_{i=1}^{10} P_i \log_2(P_i + \epsilon)$ (3)	It is possible to distinguish between the texture of an input image and a statistical measure of randomness.
Mean	$\sum_{i=1}^{N} \frac{1}{N} X_i$ (4)	The image's mean color value is the mean.
Standard Deviation	$\sqrt{\frac{1}{N}\sum_{i=1}^{N}(X_i - \text{mean})^2}$ (5)	The square root of the distribution variation is the standard deviation.
N is the total number of wave coefficients in the dataset. i is an index used in addition or iteration, describing iterations through the elements (in this case, wave coefficients) of the dataset. X_i is the i-th individual wave coefficient in the dataset. P_i is the probability of occurrence in the i-th bin of the wave coefficient histogram.		

2.6. Classifiers

Two classification techniques were employed, specifically ML and DL algorithms. In the case of ML, three algorithms were employed: K-Nearest Neighbors (KNN), Support Vector Machine (SVM), and Random Forest.

Regarding DL, two architectures were utilized, namely Convolutional Neural Network (CNN) and Artificial Neural Network (ANN). By combining these two methods, the objective of this study was to examine and comprehend the performance and benefits of each approach in the classification of alcoholic versus non-alcoholic data.

2.6.1. K-Nearest Neighbor (K-NN) K-NN method is a classification technique that utilizes data from training data to ascertain the classification of an object according to its closest distance. The KNN method yields prediction outcomes by categorizing objects based on their shortest distance from the nearest neighbor, with K representing the number of neighbors considered. This procedure entails locating the shortest distance between the assessed object and the nearest neighbor's K value in the training data [22].

Figure 4 presents a scenario where, with k set to 3 for Query B, the algorithm looks for the three nearest neighbors. The analysis revealed that among these neighbors, two belonged to class 1, and one belonged to class 0. Utilizing majority voting rules, Query B is independently assigned to class 1. Similarly, when k is set to 5 for Query A, the algorithm observes a higher number of neighbors categorized as Class 0. Consequently, Query A belongs to Class 0 [23]. The second employed algorithm was the SVM.

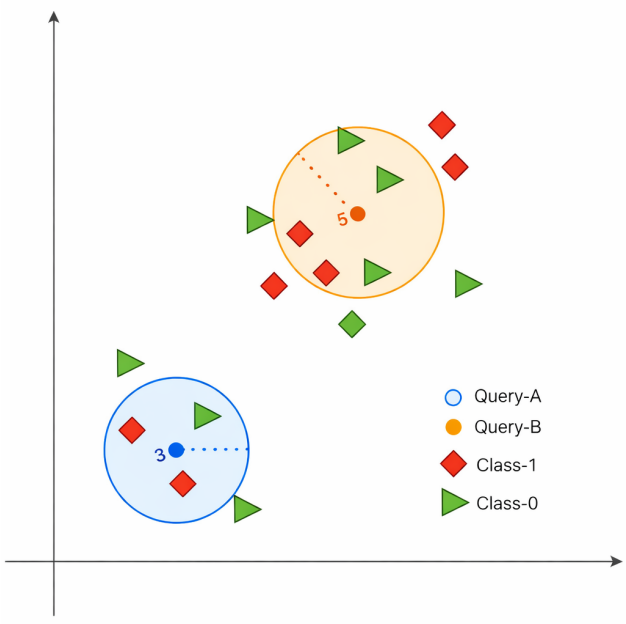


Figure 4. Illustration of k-nearest neighbors (KNN).

2.6.2. Support Vector Machine (SVM) SVM is an influential approach for constructing classifiers. The primary objective of SVM is to establish a decision boundary capable of segregating two classes, thereby enabling the prediction of labels based on one or more vector features [24]. SVM performs classification by converting the initial training data into multidimensional space and forming hyperplanes in higher dimensions. SVM is an optimal hyperplane-based mathematics learning scheme [25], as shown in Figure 5 [24].

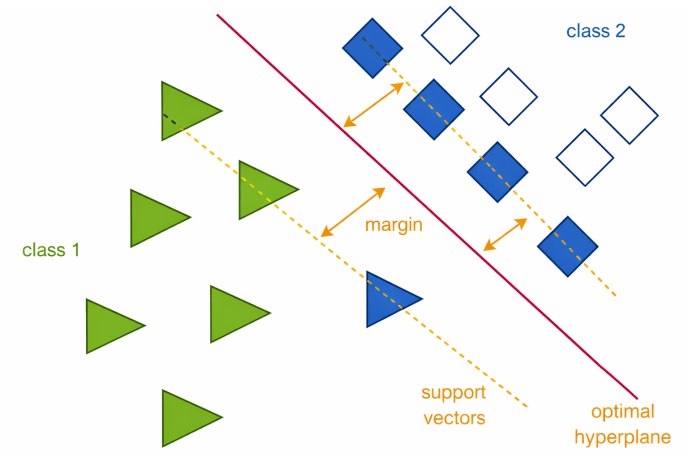


Figure 5. Optimal hyperplane in support vector machine (SVM).

SVM develops its models through a training process, just like the majority of other classifiers. SVM converts training data into nonlinear mapping functions into higher-dimensional spaces using its trick kernel. From there, data can be separated linearly or ideal hyperplanes (supporting vectors) with normalized maximal margins with respect to data points can be found. Thus, the SVM learning process aims to find the optimal linear hyperplane

in those dimensions [26]. Figure 5 shows an example of a binary class dataset separated by the SVM optimal hyperplane.

2.6.3. Random Forest (RF) Breiman introduced the RF algorithm, a tree-based ensemble learning technique made up of many decision trees. This method has been frequently used in classification and regression tasks. To increase tree diversity, RF uses a bagging approach by planting trees from bootstrap samples and randomly selecting a number of input features. In addition, by combining predictions from different decision trees, this method can effectively reduce the impact of noise in the data set and reduce overall variation in the model [27]. RF builds each tree based on bootstrap samples randomly drawn from the original dataset using the classification and regression tree (CART) and decrease Gini impurity (DGI) methods as separation criteria. When building each tree, only a limited number of randomly selected features are considered as separation candidates [26, 28].

2.6.4. Artificial Neural Network (ANN) ANN is a method used to train a network based on predetermined data and evaluate prediction results with a test dataset [29]. The working principle of this network is to imitate and model the function of the human brain in processing information and learning from experience [30]. By applying this principle, ANN can be used in computing, science, engineering, medicine, environment, agriculture, technology, business, art, and nanotechnology. This network learning process occurs through interconnected layers of artificial neurons [31].

2.6.5. Convolutional Neural Network (CNN) CNN is an ANN architecture that has been specifically crafted to cater to the requirements of image and visual processing tasks [32]. CNN effectively addresses the complexity of spatial data by utilizing convolution operations to extract local features from inputs. The structure of the CNN consists of multiple layers of convolution, non-linear activation, and pooling, which allows the formation of a hierarchy of increasingly complex features [33].

2.6.6. Implementation Details For completeness and reproducibility, the classifier hyperparameters used in this study were as follows. KNN: $k = 5$ neighbors with Euclidean distance. SVM: radial basis function (RBF) kernel with regularization parameter $C = 1.0$ and kernel coefficient $\gamma =$ "scale". Random Forest: 100 trees (estimators), with node splits determined by Gini impurity and no explicit maximum depth restriction. ANN: a fully connected feed-forward network with two hidden layers (64 and 32 units, ReLU activation) and a sigmoid output layer, trained with the Adam optimizer (learning rate 10^{-3}) and binary cross-entropy loss for 100 epochs with a batch size of 32. CNN: two convolutional blocks (32 and 64 filters, 3×3 kernels, ReLU activation, each followed by 2×2 max pooling), followed by a flattening layer, a fully connected layer of 64 units, and a sigmoid output layer, trained with the same optimizer, loss, epoch, and batch-size settings as the ANN.

2.7. Performance metrics for classification

Performance metrics in classification serve as essential instruments for assessing the efficacy and precision of machine learning classification models [34]. These metrics offer valuable insights into the model's proficiency in distinguishing between diverse classes or categories within a dataset [35]. The performance of a model can be thoroughly assessed by utilizing various metrics. These metrics include, but are not limited to, accuracy, precision, recall, specificity, F1 score, receiver operating characteristic (ROC) curves, area under the curve (AUC), confusion matrices, and classification reports. In the context of classification, accuracy is employed as a benchmark for evaluating performance, with its equation (Equation (6)) derived from the study at hand [36], where tp is the True positive, fn False negative, fp False positive, tn True negative.

$$Accuracy = \frac{tp + tn}{tp + fp + tn + fn} \tag{6}$$

3. Results

After applying the proposed design and method for AUD detection and classification, the results were provided both qualitatively and quantitatively. The time-frequency representation as well as the DWT decomposition are provided in Figure 6. Figure 6a and Figure 6b show the results of converting one-dimensional EEG signals into two-dimensional images. Using such images, the Discrete Wavelet Transform (DWT) was applied process to depict image information in a time-frequency domain at scale. In Figure 6c and Figure 6d, the level 3 wavelet tree was applied using the Db 8 mother wavelet.

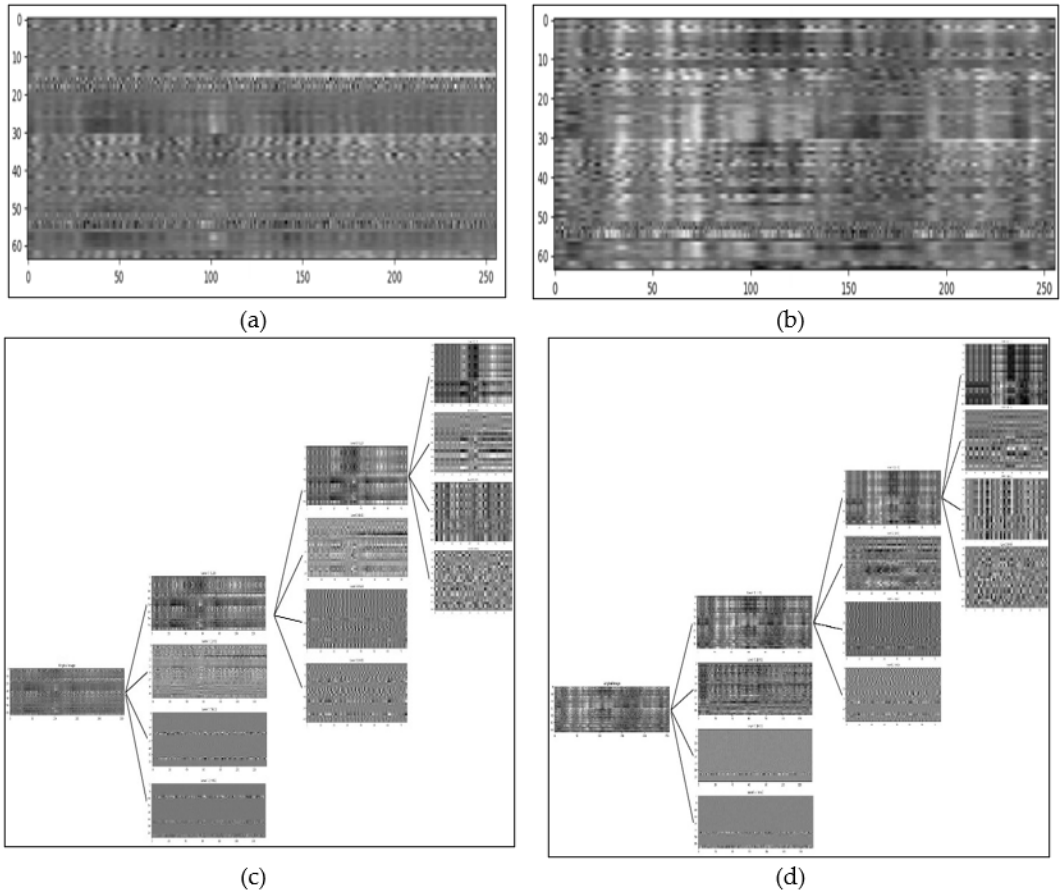


Figure 6. The Qualitative Results for AUD Detection and Classification. (a) Resulting Alcoholic image (b) Resulting Non-alcoholic image (c) DWT for alcoholic image (d) DWT for non-alcoholic image.

The comparison of the original image and the outcomes obtained by implementing DWT at level 1, level 2, and level 3 was highly evident. With each level of the DWT, there is a progressively detailed decomposition or segregation of frequency components. The visual distinctions between the original image and DWT results at various levels can provide an understanding of the time-frequency information conveyed through the WT process. Through scrutinizing these distinctions, the impact of each level of DWT on the image and discern alterations at each level were obvious.

Furthermore, results were provided as box plots and shown in Figure 7. Figure 7 illustrates feature extraction results from alcoholic EEG signals, after applying a 2D-DWT. The characteristic extraction results were Level 3 in the LL3 subband, knowing that LL contains information from low frequencies.

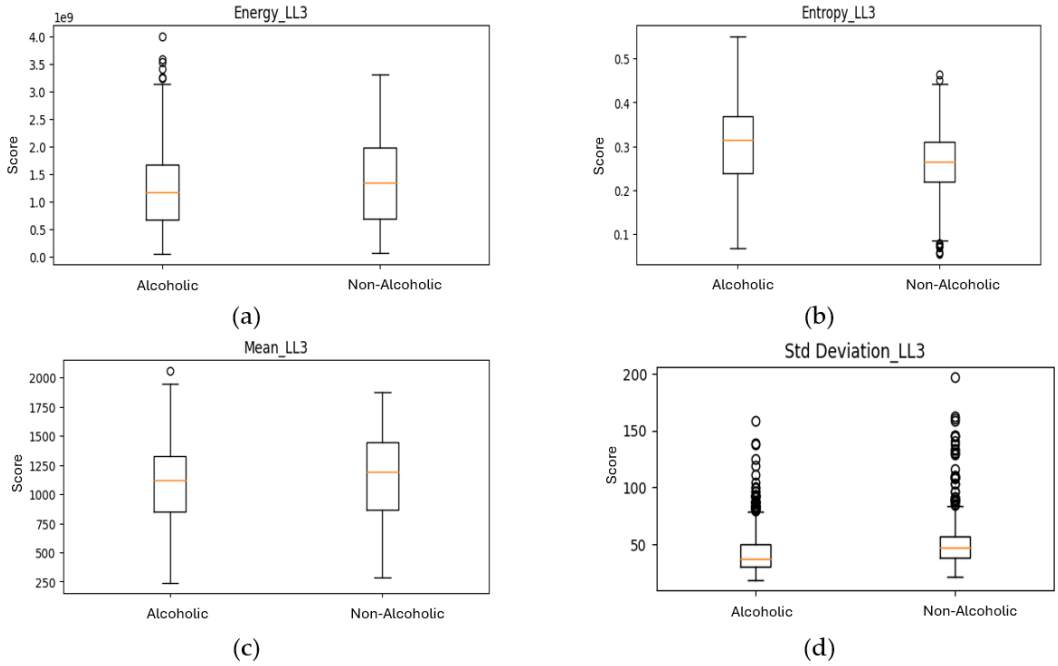


Figure 7. The features values versus the two groups of candidates (Alcoholic, non-Alcoholic). (a) LL3 energy value, (b) LL3 entropy value, (c) LL3 mean value, (d) LL3 Standard Deviation value.

The extraction results from the LL level 3 subband still overlap, hence it is not feasible in providing the best accuracy. Thus, the best features could be found in other subbands.

The classification results reported in Table 2 are based on statistical features extracted from the LL3 sub-band specifically, consistent with Figure 7. The LL3 sub-band was selected because, as the approximation coefficients at the deepest decomposition level, it concentrates the dominant low-frequency energy of the signal and yields the most compact feature representation among the ten sub-bands produced by the three-level decomposition; the remaining nine detail sub-bands (LH/HL/HH at levels 1–3) were computed but not used for the classification results reported here. As noted above, the residual overlap observed for LL3 in Figure 7 indicates that discriminative power could likely be improved by incorporating features from the detail sub-bands as well, identified here as a concrete direction for future work.

These characteristic values were further used with the classification algorithms using ML and DL. This form of classification is done using 2 data sharing scenarios. The first data distribution was carried out by training data being 50%, validation data being 30%, and testing data being 20%. The second training data was 70%, the second validation data was 20%, and the second testing data was 10%.

The two data-partitioning ratios were evaluated deliberately, rather than relying on a single fixed split, to obtain an initial indication of how sensitive the classification performance is to the proportion of available training data, with consistent accuracy trends across both scenarios taken as a simple stability check. Repeated k-fold cross-validation would provide a more statistically robust estimate of generalization performance than hold-out splits, particularly for a dataset of this size. Adopting a cross-validated evaluation protocol, together with subject-wise fold construction to guard against leakage between trials of the same subject, is planned as a priority extension of this work.

The quantitative results summarized in Table 2 reveal several important observations regarding feature effectiveness and classifier behavior.

First, energy consistently outperforms other statistical features across almost all classification models, particularly when combined with ensemble-based approaches. The best overall performance, achieving 93.77% accuracy, is obtained using the energy feature with the Random Forest (RF) classifier under the 70%–20%–10%

data split. This indicates that energy-based representations are highly discriminative for capturing alcohol-related EEG patterns, especially in the low-frequency components emphasized by the LL sub-band.

Second, mean-based features consistently yield the lowest accuracy across classifiers, with the poorest result (51.26%) observed for SVM. This suggests that the mean value alone is insufficient to characterize the complex temporal–frequency variations present in multichannel EEG signals and provides limited class-separating information.

Third, combining all extracted features does not necessarily improve classification performance. In several cases, the "All Features" configuration performs comparably or even worse than single-feature setups. This behavior indicates potential feature redundancy and scale dominance, particularly from the energy feature, which may mask the contribution of other statistical descriptors.

Regarding classifier performance, Random Forest demonstrates the most robust and stable behavior across different feature sets and data partitions, outperforming KNN and SVM in most cases. This can be attributed to its ensemble learning mechanism, which effectively handles feature interactions and mitigates overfitting.

In contrast, deep learning models (ANN and CNN) show inferior performance, particularly when trained on handcrafted statistical features. This outcome is mainly due to the limited dataset size, the absence of data augmentation, and the non end-to-end learning setup, conditions under which classical machine learning methods are known to be more effective.

Fourth, it should be noted that the accuracy values reported in Table 2 are obtained from single hold-out evaluations rather than repeated resampling; consequently, the differences between classifiers (e.g., between Random Forest and ANN/SVM under the Standard Deviation feature) are not yet supported by formal statistical significance testing. Given how close several of the top-performing configurations are, the present accuracy comparison should be regarded as indicative rather than conclusive. Formal hypothesis testing (e.g., a paired t-test or Wilcoxon signed-rank test computed over cross-validation folds) is identified as necessary future work to substantiate the claim that Random Forest is significantly superior to the alternative models.

Fifth, accuracy is reported as the primary evaluation metric in this study, consistent with Equation (6). For a medical screening task such as AUD detection, precision, recall, specificity, F1-score, and confusion-matrix-based error analysis provide additional, clinically relevant information, for example about the relative rate of false negatives versus false positives, that accuracy alone does not capture, particularly if the underlying classes are not perfectly balanced. Reporting the full set of classification metrics, together with an analysis of which samples are consistently misclassified across classifiers, is planned as part of the more rigorous, cross-validated evaluation described above.

4. Discussion

The proposed approach provided 93.77% accuracy in AUD detection and classification using the energy feature. In this classification, the accuracy value of All Features does not produce significant results. This is because the energy value is too large, however, there is an overlap in other features.

As DL gave the poorest results of AUD detection, this is due to the fact that DL is recommended for direct image classification [37] and requires more data [38]. Noteworthy that this study did not use augmentation to change the form of the data.

In the present study, CNN and ANN were deliberately trained on the same handcrafted statistical features (Energy, Entropy, Mean, Standard Deviation) as the machine learning classifiers, rather than directly on the 2D wavelet sub-band images, so that the input representation would be identical across all five classifiers and allow a controlled comparison of classifier behavior on a common feature space. This design choice, however, does not let the CNN exploit its principal strength, namely automatic hierarchical feature learning from raw or minimally processed image data, and is a likely explanation for its comparatively weak performance here rather than an intrinsic limitation of CNNs for this problem. An end-to-end CNN applied directly to the 2D wavelet sub-band images, combined with data augmentation strategies to compensate for the limited number of subjects, is a direct and promising extension of this work and is left for future study.

Table 2. The Accuracy Results of AUD Detection and Classification.

No.	Method	Feature	Accuracy (%) Train 50, Val 30, Test 20	Accuracy (%) Train 70, Val 20, Test 10
1	KNN	Energy	76.25	80.67
		Entropy	77.08	84.87
		Mean	57.08	57.14
		Standard Deviation	83.33	**93.28**
		All Features Without Mean	82.83	88.24
		All Features	82.35	77.50
2	SVM	Energy	74.17	**79.83**
		Entropy	66.25	72.72
		Mean	46.67	51.26
		Standard Deviation	76.67	78.99
		All Features Without Mean	75.83	78.99
		All Features	76.66	77.31
3	RF	Energy	85.50	**93.77**
		Entropy	75.64	77.61
		Mean	60.66	64.87
		Standard Deviation	85.81	92.44
		All Features Without Mean	84.41	92.84
		All Features	85.41	90.75
4	ANN	Energy	86.25	87.39
		Entropy	74.58	80.67
		Mean	55.83	61.34
		Standard Deviation	86.25	**92.44**
		All Features Without Mean	80.83	82.50
		All Features	78.81	83.99
5	CNN	Energy	82.99	86.01
		Entropy	76.67	81.51
		Mean	57.50	61.34
		Standard Deviation	85.00	**90.76**
		All Features Without Mean	80.83	86.55
		All Features	79.83	87.25

A comparative analysis showcasing the different accuracy values obtained in the literature versus the accuracy achieved in the exploratory work for the detection of AUD is represented in Table 3.

Noteworthy that in previous research [1, 7, 8, 9], the decomposition process was carried out on each channel in the EEG signal. Unlike the current exploratory research conducted. Although the accuracy in [1] and [8] was a bit higher, in the current research, N channels were considered as an image so that 2D-DWT can be applied. This provides several advantages, such as, the required computing time is quite short and more flexible as compared to other techniques. Moreover, the resulting accuracy is quite competitive with other methods.

From an algorithmic standpoint, representing the N-channel EEG signal as a single 2D array and decomposing it with one 2D-DWT operation requires only a single wavelet-transform call per trial, whereas conventional channel-wise 1D-DWT approaches require the decomposition to be repeated once per channel (i.e., up to $N = 64$ calls per trial for the present dataset). This analytical argument supports the expectation of reduced computational overhead for the proposed approach. The comparison presented here is a theoretical computational-complexity argument rather than an empirically measured one, as wall-clock runtime against a channel-wise 1D-DWT baseline on identical hardware has not yet been benchmarked. A direct empirical timing comparison against 1D-DWT pipelines is planned as part of a future, more comprehensive validation of this work.

Table 3. Comparison results with previous research on wavelet use with classification algorithms.

Ref	Dataset	Wavelet used	Features Extraction	Classifier	Acc (%)
[1]	UCI Machine Learning Repository	Flexible analytic wavelet transforms	–	Least square-support vector machine (LS-SVM), Support vectors machine (SVM), Naïve Bayes, Performance metrics	99.16
[7]	Primary Dataset	Discrete Wavelet Transform (Db 7)	Minimum, Maximum, Average, Kurtosis, Mean square, and Standard deviation	boosted trees, SVM, neural networks, and decision trees	95.6
[8]	UCI Machine Learning Repository	Dual-Tree Complex Wavelet Transform	L2Ns and LEEs	SVM, Fuzzy Sugeno Classifier (FSC)	97.91
[9]	UCI Machine Learning Repository	Discrete Wavelet Transform (Haar, Db2, Db8, Bior1.5, and Bior2.8, Level1-7)	MWPE	SVM	77.8
Proposed Work	UCI Machine Learning Repository	Discrete Wavelet Transform 2D	Statistical Features	KNN, SVM, Random Forest, ANN, and CNN	93.77

The promising result of this research provides an opportunity to conduct further exploration of 2D-DWT. A deeper study of mother wavelet selection and decomposition levels in 2D-DWT is expected to improve the accuracy.

Two prior studies in Table 3, namely [1] (99.16%) and [8] (97.91%), report higher accuracy than the proposed method. The contribution of the present work lies not in surpassing the absolute accuracy of the state of the art, but in demonstrating a computationally simpler alternative: a single joint 2D-DWT decomposition of all channels, rather than channel-wise decomposition or the least-square/flexible-wavelet formulations used in [1, 8], still achieves competitive accuracy (93.77%) while requiring substantially fewer wavelet-transform operations (Section 4, computational-cost discussion above). The methods in [1] and [8] employ specialized wavelet formulations, flexible analytic wavelet transform and dual-tree complex wavelet transform respectively, that are individually more sophisticated than the standard 2D-DWT used here. Combining such formulations with the proposed joint multichannel representation is a promising direction for future work that may close the remaining accuracy gap. A direct, controlled ablation comparing the proposed joint 2D-DWT representation against channel-wise 1D-DWT under an identical feature-extraction and classification pipeline, to isolate the specific contribution of the 2D joint representation, was not performed in the present study and is identified as a priority for future work.

Beyond wavelet-based 2D representations, other approaches to converting multichannel EEG into a 2D or image-like form exist in the literature, such as topographic scalp maps, time–frequency spectrograms per channel, and inter-channel connectivity matrices; a systematic comparison of the proposed channel-stacked representation against these alternatives was outside the scope of the present study and is left for future work.

From a translational perspective, an automated AUD screening tool based on routinely acquired EEG recordings could, in principle, support clinicians as a low-cost, non-invasive adjunct to existing behavioral and self-report

screening instruments; realizing this potential, however, would require validation on independent, subject-disjoint, and ideally multi-site cohorts, together with the statistical rigor discussed above, before any clinical utility claim can be made. The present study should be regarded as a methodological proof of concept rather than a clinically validated screening tool.

5. Conclusions

This study applied the 2D-DWT associated with ML and DL algorithms method to detect AUD and classify EEG signals into Alcoholic and Non-Alcoholic. The first step involves the conversion of an N-channels EEG signal into a 2D format, enabling it to be processed as a general image. In this scenario, the DWT algorithm was employed, by utilizing the Db 8 mother wavelet. Also included conducting a 3-level decomposition, resulting in the production of 10 sub-bands. Each subband was extracted using statistical features and then advanced with classification using machine learning and deep learning.

After the exploration and experiments done on real EEG signals and after the implementation of the Random Forest technique, AUD detection yielded a remarkable accuracy rate of 93.77%, rendering it the most preferable method when compared to alternative classification methodologies.

Further exploration can apply changes to the mother wavelet type and add experiments to several other wavelet subbands. Moreover, more ML and DL algorithms can be involved for future exploration.

In particular, priority directions for future work include: (i) evaluating the pipeline under repeated k-fold, subject-wise cross-validation with formal statistical significance testing (e.g., paired t-test or Wilcoxon signed-rank test) to substantiate classifier comparisons, and reporting the full set of classification metrics (precision, recall, specificity, F1-score) together with confusion-matrix-based error analysis; (ii) constructing a topographically faithful 2D representation of the EEG channels, e.g., via spherical-spline interpolation, to explicitly incorporate scalp spatial priors into the 2D-DWT decomposition, and comparing it against alternative 2D representations (topographic maps, spectrograms, connectivity matrices); (iii) training an end-to-end CNN directly on the 2D wavelet sub-band images together with data augmentation; (iv) empirically benchmarking the computational runtime of the proposed 2D-DWT pipeline against channel-wise 1D-DWT baselines, including a controlled ablation isolating the specific contribution of the joint 2D representation; and (v) analyzing channel importance, e.g., via per-channel ablation or feature-importance scores, to identify which of the 64 EEG channels contribute most to classification performance and to guide channel selection in future work.

Author Contributions

Conceptualization, A.R. and D.B.; methodology, A.R and I.W.; software, D.B.; validation, A.R., D.B. and A.Z.; formal analysis, A.R. A.Z.; investigation, D.B. and I.W; resources, D.B.; data curation, A.R. and I.W; writing—original draft preparation, A.R. and D.B.; writing—review and editing, A.Z. and I.W; visualization, D.B.; supervision, A.Z. All authors have read and agreed to the published version of the manuscript.

Data Availability Statement

Data used to support the findings of this study are available from open databases (http://archive.ics.uci.edu/dataset/121/eeg+database).

Acknowledgement

The authors would like to thank Telkom University for providing research facilities and technical support. The authors also acknowledge the use of the UCI Machine Learning Repository for providing the EEG dataset used in this study.

Conflicts of Interest

The authors declare no conflicts of interest.

Abbreviations

The following abbreviations are used in this manuscript:

AUD	Alcohol Use Disorder
EEG	Electroencephalogram
WHO	World Health Organization
WT	Wavelet Transformation
DWT	Discrete Wavelet Transform
2D/1D	Two-/One-Dimensional
ML	Machine Learning
DL	Deep Learning
KNN	K-Nearest Neighbors
SVM	Support Vector Machine
RF	Random Forest
ANN	Artificial Neural Network
CNN	Convolutional Neural Network
CART	Classification and Regression Tree
DGI	Decrease Gini Impurity
ROC	Receiver Operating Characteristic
AUC	Area Under the Curve
UCI	University of California, Irvine
MWPE	Multilevel Wavelet Packet Entropy
GLDM	Grey Level Differences Matrix
NGBoost	Natural Gradient Boosting
L2Ns	L2-Norms
LEEs	Log-Energy Entropies
LL/LH/HL/HH	Approximation / Horizontal / Vertical / Diagonal DWT Sub-bands
PCA	Principal Component Analysis
RFE	Recursive Feature Elimination

REFERENCES

1. A. Anuragi, and D. Singh Sisodia, *Alcohol use disorder detection using EEG signal features and flexible analytical wavelet transform*, Biomedical Signal Processing and Control, vol. 52, pp. 384–393, 2019.
2. World Health Organization, *Global Status Report on Alcohol and Health 2018*, World Health Organization, Switzerland, 2018.
3. World Health Organization, *Global Strategy to Reduce the Harmful Use of Alcohol*, World Health Organization, 2010.
4. A. Priya, P. Yadav, S. Jain, and V. Bajaj, *Efficient method for classification of alcoholic and normal EEG signals using EMD*, The Journal of Engineering, vol. 2018, pp. 166–172, 2018.

5. R.M. Aileni, S. Pasca, and A. Florescu, *EEG-brain activity monitoring and predictive analysis of signals using artificial neural networks*, Sensors, vol. 20, p. 3346, 2020.
6. H. Jebelli, S. Hwang, and S. Lee, *EEG signal-processing framework to obtain high-quality brain waves from an off-the-shelf wearable EEG device*, Journal of Computing in Civil Engineering, vol. 32, 2018.
7. A.A. Kawthar, D. Mark, A. Mia, Z. Amira, K. Fadi, and N. Ziad, *Seizure initiation with focal electrically administered seizure therapy (FEAST)*, Neuropsychopharmacology, vol. 40, pp. S443–S611, 2015.
8. A. Teddy, D. Mark, Z. Amira, K. Fadi, and N. Ziad, *Contrasting non-linear dynamic analyses of EEG in alert and sedated states*, Neuropsychopharmacology, vol. 40, pp. S106–S271, 2015.
9. C. Ekaputri, R. Widadi, and A. Rizal, *EEG signal classification for alcoholic and non-alcoholic person using multilevel wavelet packet entropy and support vector machine*, in Proceedings of the 2020 8th International Conference on Information and Communication Technology (ICoICT), IEEE, pp. 1–4, June 2020.
10. D.S. Beu, H.H. Simatupang, A. Rizal, R. Purnamasari, and Y.N. Fuadah, *Classification EEG signal using texture analysis and artificial neural network for alcoholic detection*, pp. 53–62, 2024.
11. D.T. Barus, F. Masri, and A. Rizal, *NGBoost interpretation using LIME for alcoholic EEG signal based on GLDM feature extraction*, pp. 894–904, 2020.
12. X.L. Zhang, H. Begleiter, B. Porjesz, W. Wang, and A. Litke, *Event related potentials during object recognition tasks*, Brain Research Bulletin, vol. 38, pp. 531–538, 1995.
13. UCI Machine Learning Repository, *EEG Database Data Set*, http://archive.ics.uci.edu/dataset/121/eeg+database, accessed 2026.
14. B. Sri Aprillia, A. Rizal, and M.A. Geraldy Fauzi, *Grey level differences matrix for alcoholic EEG signal classification*, JOIV: International Journal on Informatics Visualization, vol. 8, p. 26, 2024.
15. P. Garg, and R.R. Kishore, *An efficient and secured blind image watermarking using ABC optimization in DWT and DCT domain*, Multimedia Tools and Applications, vol. 81, pp. 36947–36964, 2022.
16. R. Ashraf, M. Ahmed, S. Jabbar, S. Khalid, A. Ahmad, S. Din, and G. Jeon, *Content based image retrieval by using color descriptor and discrete wavelet transform*, Journal of Medical Systems, vol. 42, p. 44, 2018.
17. A.M. Abdulazeez, D.Q. Zeebaree, D.A. Zebari, G.M. Zebari, and I.M.N. Adeen, *The applications of discrete wavelet transform in image processing: A review*, Journal of Soft Computing and Data Mining, vol. 1, pp. 31–43, 2020.
18. M. Zhu, Y. Yang, X. Feng, Z. Du, and J. Yang, *Robust modeling method for thermal error of CNC machine tools based on random forest algorithm*, Journal of Intelligent Manufacturing, vol. 34, pp. 2013–2026, 2023.
19. R. Zebari, A. Abdulazeez, D. Zeebaree, D. Zebari, and J. Saeed, *A comprehensive review of dimensionality reduction techniques for feature selection and feature extraction*, Journal of Applied Science and Technology Trends, vol. 1, pp. 56–70, 2020.
20. A.J. Zaylaa, A. Harb, F.I. Khatib, Z. Nahas, and F.N. Karameh, *Entropy complexity analysis of electroencephalographic signals during pre-ictal, seizure and post-ictal brain events*, in Proceedings of the 2015 International Conference on Advances in Biomedical Engineering (ICABME), IEEE, pp. 134–137, September 2015.
21. W.K. Mutlag, S.K. Ali, Z.M. Aydam, and B.H. Taher, *Feature extraction methods: A review*, Journal of Physics: Conference Series, vol. 1591, p. 012028, 2020.
22. A. Nurdina, and A.B.I. Puspita, *Naive Bayes and KNN for airline passenger satisfaction classification: Comparative analysis*, Journal of Information System Exploration and Research, vol. 1, 2023.
23. S. Uddin, I. Haque, H. Lu, M.A. Moni, and E. Gide, *Comparative performance analysis of K-nearest neighbour (KNN) algorithm and its different variants for disease prediction*, Scientific Reports, vol. 12, p. 6256, 2022.
24. A.J. Zaylaa, A. Daher, M. Ayache, N. Omeirat, R. Mahmoud, and B.A. Hawili, *Early diagnosis of osteoporosis: An artificial intelligence-based framework*, in Proceedings of the 2023 Seventh International Conference on Advances in Biomedical Engineering (ICABME), IEEE, pp. 226–231, October 2023.
25. M.A. Chandra, and S.S. Bedi, *Survey on SVM and their application in image classification*, International Journal of Information Technology, vol. 13, pp. 1–11, 2021.
26. H. Faris, M.A. Hassonah, A.M. Al-Zoubi, S. Mirjalili, and I. Aljarah, *A multi-verse optimizer approach for feature selection and optimizing SVM parameters based on a robust system architecture*, Neural Computing and Applications, vol. 30, pp. 2355–2369, 2018.
27. M. Zhu, Y. Yang, X. Feng, Z. Du, and J. Yang, *Robust modeling method for thermal error of CNC machine tools based on random forest algorithm*, Journal of Intelligent Manufacturing, vol. 34, pp. 2013–2026, 2023.
28. M. Sewak, *Policy-based reinforcement learning approaches*, in Deep Reinforcement Learning, Springer Singapore, Singapore, pp. 127–140, 2019.
29. O.I. Abiodun, A. Jantan, A.E. Omolara, K.V. Dada, N.A. Mohamed, and H. Arshad, *State-of-the-art in artificial neural network applications: A survey*, Heliyon, vol. 4, p. e00938, 2018.
30. M.M. Saritas, and A. Yasar, *Performance analysis of ANN and Naive Bayes classification algorithm for data classification*, International Journal of Intelligent Systems and Applications in Engineering, vol. 7, pp. 88–91, 2019.
31. H. Moayedi, M. Mehrabi, M. Mosallanezhad, A.S.A. Rashid, and B. Pradhan, *Modification of landslide susceptibility mapping using optimized PSO-ANN technique*, Engineering with Computers, vol. 35, pp. 967–984, 2019.
32. D. Bhatt, C. Patel, H. Talsania, J. Patel, R. Vaghela, S. Pandya, K. Modi, and H. Ghayvat, *CNN variants for computer vision: History, architecture, application, challenges and future scope*, Electronics, vol. 10, p. 2470, 2021.
33. A. K, D.R.V. P M, K. Srinivasan, and C.-Y. Chang, *Deep convolutional neural network based feature extraction with optimized machine learning classifier in infant cry classification*, in Proceedings of the 2020 International Conference on Decision Aid Sciences and Application (DASA), IEEE, pp. 27–32, November 2020.
34. A. Luque, A. Carrasco, A. Martín, and A. de las Heras, *The impact of class imbalance in classification performance metrics based on the binary confusion matrix*, Pattern Recognition, vol. 91, pp. 216–231, 2019.
35. M. Grandini, E. Bagli, and G. Visani, *Metrics for multi-class classification: An overview*, 2020.

36. H. M, and S. M.N, *A review on evaluation metrics for data classification evaluations*, International Journal of Data Mining & Knowledge Management Process, vol. 5, pp. 01–11, 2015.
37. D. Han, Q. Liu, and W. Fan, *A new image classification method using CNN transfer learning and web data augmentation*, Expert Systems with Applications, vol. 95, pp. 43–56, 2018.
38. S.R. Waheed, M.S.M. Rahim, N.M. Suaib, and A.A. Salim, *CNN deep learning-based image to vector depiction*, Multimedia Tools and Applications, vol. 82, pp. 20283–20302, 2023.